Molecular Recognition in Purinergic Receptors. 2. Diastereoselectivity of the *h*-P2Y$_1$-Receptor†

Dan T. Major,‡ Victoria Nahum,‡ Yingfei Wang,§ Georg Reiser,§ and Bilha Fischer*,‡

Department of Chemistry, Gonda-Goldschmied Medical Research Center, Bar-Ilan University, Ramat-Gan 52900, Israel, and Institute for Neurobiochemistry, Faculty of Medicine, Otto von Guericke University, Leipziger Str. 44 D-39120 Magdeburg, Germany

Received March 24, 2004

In the companion paper, part 1, we described the construction of an improved molecular model for the *h*-P2Y$_1$ receptor (*h*-P2Y$_1$-R) and proposed a rational for the stereoelectronic selectivity of the receptor. Here, we extend our studies on the molecular recognition of the *h*-P2Y$_1$-R to the exploration of the diastereoselectivity of this receptor. For this purpose, we implemented an integrative approach combining synthesis, spectral analysis, biochemical assays, and computational analysis. Specifically, we selected and synthesized novel ATP analogues bearing a chiral center on the phosphate chain. We analyzed the conformation of the chiral ATP analogues in solution by ^{1}H/^{13}C NMR and assigned the absolute configuration of the diastereoisomers. The coordination mode of these analogues with a Mg^{2+} ion was evaluated by ^{31}P NMR. These chiral analogues were biochemically evaluated and found to be potent *h*-P2Y$_1$-R ligands. An EC$_{50}$ difference of ca. 20-fold was observed between the diastereoisomers. Their spectral absolute configuration assignment was confirmed by comparison of the biochemical results to those of ATP-α-S diastereoisomers whose chirality is known. Finally, a computational analysis was performed for the elucidation of molecular recognition employing molecular mechanics (docking) studies on the receptor:ligands complexes. On the basis of the current results, we hypothesize that *h*-P2Y$_1$-R's chiral discrimination originates from the requirement that the nucleotide analogue interacts with a Mg^{2+} ion within the receptor binding site. This Mg^{2+} ion is possibly coordinated with both Asp204 and the ATP's α, *β*, *γ*-phosphates in a Λ configuration.

Introduction

Studies of the molecular recognition of ATP receptors (P2-Rs), and especially of the P2Y$_1$-R subtype, have focused over the past decade on the stereoelectronic requirements of the receptors. The question of the molecular recognition of the P2Y$_1$-R was addressed by SAR studies of novel ATP analogues,[1] site-directed mutagenesis, and molecular modeling.[2]

However, to the best of our knowledge, the question of the receptor's diastereoselectivity has not been addressed. The need for addressing this question arose as we discovered that the P2Y$_1$-R demonstrates a clear preference for one of the diastereoisomers of our chiral P$_\alpha$-phosphate ATP ligands (Scheme 1). These ligands include ATP-α-B analogues (**3**, **4**, **7**, **8**, **11**, **12**)[3] and ATP-α-S analogues (**5**, **6**, **9**, **10**) (described below). Studies of this chiral selectivity are expected both to provide the origin of the receptor's diastereoselectivity and to help design novel potent and selective agonists.

For elucidating the origin of the receptor's chiral discrimination, we implemented the following strategy: (1) synthesis and separation of the P$_\alpha$-chiral-ATP analogues, (2) biochemical analysis of the pure diastereoisomers of analogues **3**−**12** as P2Y$_1$-R ligands, (3) conformational analysis of one of the diastereoisomeric pairs in solution and elucidation of the absolute configuration around the P$_\alpha$ in analogues **3**−**12**, and (4) docking studies of the diastereoisomeric pairs of analogues **3**−**12** at the P2Y$_1$-R binding-site, as obtained by molecular modeling (preceding companion paper),[4] in order to reveal the origin of chiral selectivity of the P2Y$_1$-R.

Scheme 1. ATP Analogues Used as Stereo- and Diastereoprobes of the P2Y$_1$-R

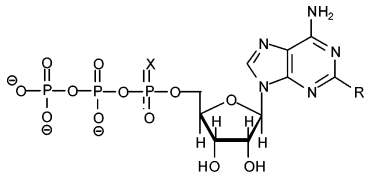

1. R = H, X = O
2. R = SMe, X = O
3. R = H, X = BH_3^- (Rp)
4. R = H, X = BH_3^- (Sp)
5. R = H, X = S (Sp)
6. R = H, X = S (Rp)
7. R = SMe, X = BH_3^- (Rp)
8. R = SMe, X = BH_3^- (Sp)
9. R = SMe, X = S (Sp)
10. R = SMe, X = S (Rp)
11. R = Cl, X = BH_3^- (Rp)
12. R = Cl, X = BH_3^- (Sp)

Here, we report on the identification of the preferred P2Y$_1$-R ligands' diastereoisomers and their absolute configuration and propose explanations for the receptor's diastereoselectivity.

Results

Selection and Preparation of ATP Analogues for Probing Chiral Discrimination of the *h*-P2Y$_1$-R.

† This work has been supported by Innodia Inc, Montreal, Canada.
* Corresponding author. Fax: 972−3−5351250. Tel: 972−3−5318303. E-mail: bfischer@mail.biu.ac.il.
‡ Bar-Ilan University.
§ Otto von Guericke University.

10.1021/jm049771u CCC: $27.50
Published on Web 08/03/2004

Scheme 2. Substitution of Nonbonding Oxygen on P_α by BH_3 Group or Sulfur Atom Induces the Formation of S_p and R_p Distereoisomers

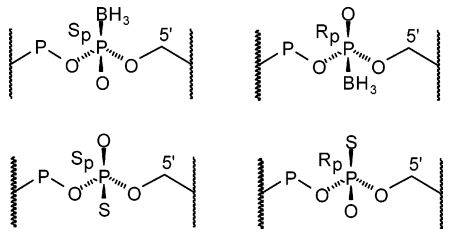

Phosphorothioate analogues of ATP have been widely used for the determination of the stereoselectivity of enzymes and the configuration of the metal−ATP substrate complex in enzymatic reactions by measuring kinetic parameters of the enzymatic reaction with the diastereoisomers of ATP-α-S and ATP-β-S in the presence of various metal ions.[5]

For probing the chiral discrimination of the *h*-$P2Y_1$-R, we chose ATP analogues **3**−**12** possessing a chiral P_α (Scheme 2).

In previous studies, we synthesized various ATP-α-S analogues and established their $P2Y_1$-R affinity.[6] Therefore, we applied ATP-α-S analogues **5/6** and **9/10**, established in this study to possess $P2Y_1$-R affinity, as probes for exploring the chiral discrimination of $P2Y_1$-R. For this purpose, we also applied ATP-α-B probes **3/4**, **7/8**, and **11/12**, which we recently synthesized and characterized as potent $P2Y_1$-R ligands.[3] Furthermore, these ATP-α-B analogues show no potency at the $P2Y_2$-receptor.[7]

The diastereoisomeric pair of 2-MeS-ATP-α-S analogues **9/10** was prepared here in two steps from 2-SH-adenosine. Highly facile and selective S-alkylation afforded 2-MeS-adenosine in quantitative yield. This derivative was then triphosphorylated in a one-pot reaction[6] to afford the product as a diastereomeric pair **9/10** (Scheme 3). The products were analyzed by ^1H and ^{31}P NMR spectra (Figure 1) and the diastereoisomers were separated by HPLC (Figure 2).

Finally, for the comparison of $P2Y_1$-R affinity of analogues **9/10** to the parent compound and for establishing the absolute configuration of analogues **9/10**, we also biochemically assayed commercial ATP-α-S R_p and S_p diastereoisomers **5/6**.

Conformational Analysis of 2-MeS-ATP-α-B in Solution and Assignment of Absolute Configuration of the Chiral Probes. Adenine nucleotides are expected to possess conformational flexibility, due to possible rotations around the glycosidic bond and pseudorotation of the ribose ring, as well as possible rotations around the C4′−C5′, C5′−O5′, and O5′−P_α bonds.

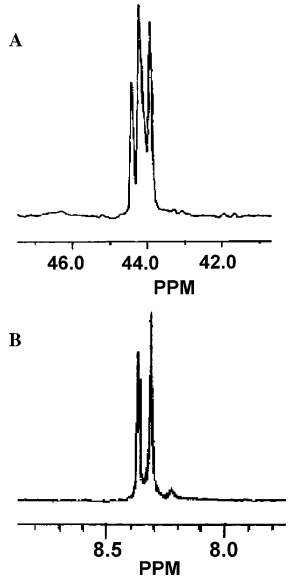

Figure 1. NMR spectra of 2-MeS-ATP-α-S (mixture of two diastereoisomers): (A) ^{31}P NMR spectrum. Signals of P_α of R_p- and S_p-isomers measured at 81 MHz. (B) ^1H NMR spectrum. Signals of H8 of R_p- and S_p-isomers measured at 200 MHz.

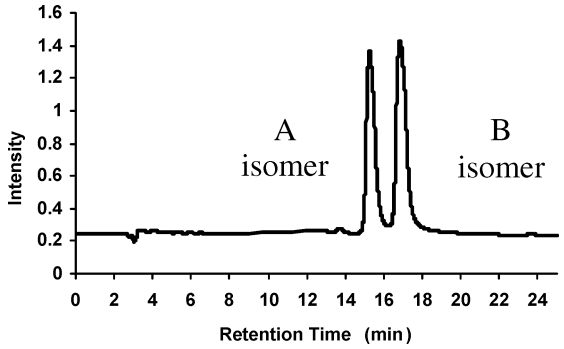

Figure 2. HPLC chromatogram of a mixture of 2-MeS-ATP-α-S diastereoisomers **9**,**10**. Separation was performed on a LichroCART LiChrospher 60 RP-select B column (250 × 10 mm), flow rate 5 mL/min. A linear gradient of methanol:0.1 M triethylammonium acetate, 10:90 to 30:70, in 25 min was applied.

Scheme 3. Preparation of Chiral Probes **9/10**

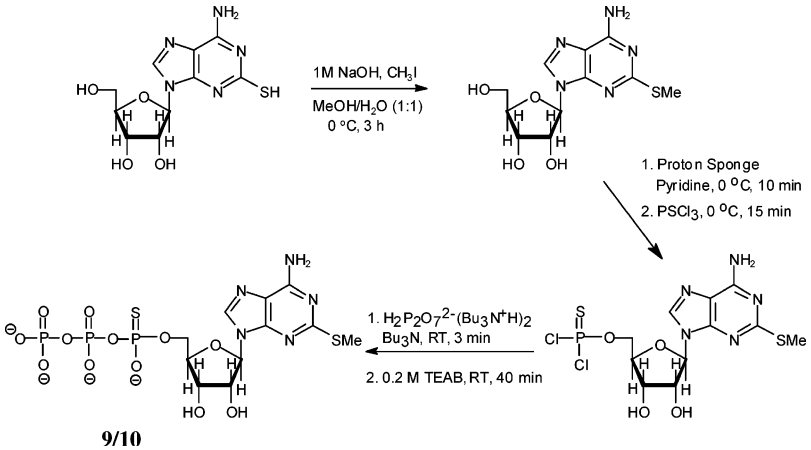

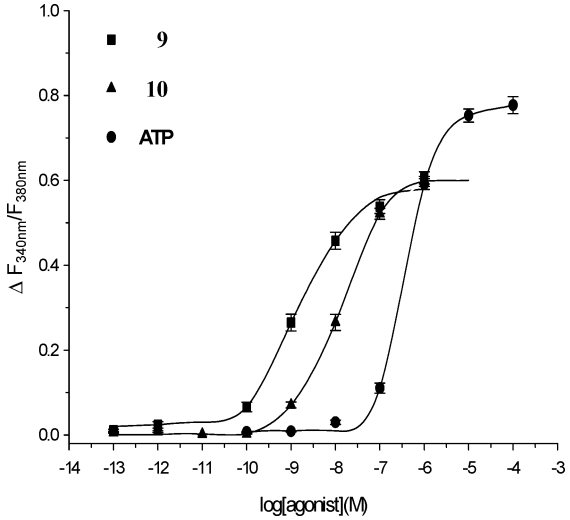

Figure 3. Concentration−response curves for **9**,**10** isomers and ATP by measuring intracellular calcium ($[Ca^{2+}]_i$) mobilization in HEK cells expressing the $P2Y_1$ receptor. Black squares, triangles, and circles represent the concentration−response curves for **9**, **10**, and ATP, respectively. The data points represent the mean ± SEM of 57-220 cells from at least three different experiments and three different cells preparations.

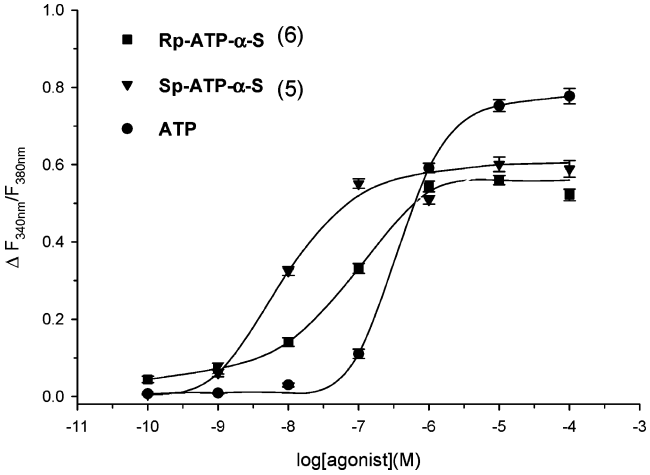

Figure 4. Concentration−response curves for R_p-ATP-α-S (**6**), S_p-ATP-α-S (**5**), and ATP by measuring intracellular calcium ($[Ca^{2+}]_i$) mobilization in HEK cells expressing the $P2Y_1$ receptor. Black squares, triangles, and circles represent the concentration−response curve for R_p-ATP-α-S, S_p-ATP-α-S, and ATP, respectively. The data points represent the mean ± SEM of 64-220 cells from at least three different experiments and three different cells preparations.

However, it is well-established that most 5′-nucleotides adopt a predominant preferred conformation in solution (which is nevertheless in equilibrium with other conformations).[8]

Thus, it has been shown that a majority of purine and pyrimidine 5-nucleotides favor an anti conformation of base ring with respect to the sugar ring.[9] Likewise, the ribose ring exhibits a puckered conformation in which either the C2′ or C3′ atom is furthest from the plane of the other atoms of the ribose ring, named as South (*S*) and North (*N*) conformations, respectively.[10] Finally, it has been shown that the ribose exocyclic group exists predominantly in a gauche−gauche (*gg*) conformation about the C4′−C5′ bond, with the O5′ atom projecting over the furanose ring.

Analysis of Spectra. Here, we employed ^1H and ^{13}C NMR spectra to study the solution conformation of both diastereoisomers of 2-MeS-ATP-α-B, **7**/**8**, and to elucidate the absolute configuration around P_α for both diastereoisomers. This absolute configuration assignment enabled also the assignment of chirality of the other probes under investigation. The chemical shifts and splitting pattern of adenine and sugar protons of 0.03 M D_2O solutions of both diastereoisomers of 2-MeS-ATP-α-B were assigned from ^1H NMR spectra at 300 and 600 MHz (Tables 1 and 2). Diastereoisomers **7** and **8** were denoted as A and B, respectively, where the A-isomer is the first eluting isomer from HPLC.

Conformation Around the Glycosidic Bond. Purine nucleotides can adopt two main conformations, syn or anti, in which the aromatic proton H8 points above or away from the sugar ring. The quantitative determination of the conformation around the glycosidic bond can be obtained by monitoring the vicinal coupling constants $^3J_{C8-H1'}$ and $^3J_{C4-H1'}$, which are extracted from ^{13}C NMR spectra for each diastereomer of **7** and **8**. A practical rule for the orientation of the base relative to the ribose was formulated: a value of $^3J_{C4-H1'} < {}^3J_{C8-H1'}$ indicates that χ is in the anti conformation, whereas the reverse indicates that χ is in the syn conformation.[11] The *J*-coupling constants in Table 2 provide strong support for the preferred anti-conformer in solution for both diastereoisomers of 2-MeS-ATP-α-B.

The magnitude of a three-bond scalar coupling *J* depends on the value of the corresponding torsion angle θ by the following expression, which is known as the Karplus equation:

$$^3J(\theta) = A\cos^2\theta + B\cos\theta + C$$

Ippel et al. reparametrized and generalized the Karplus equations for the glycosidic bond conformation of purine and pyrimidine nucleosides and nucleotides.[11]

The following equations[11] were used in this study to calculate the glycosidic bond angle χ for A- and B-isomers of 2-MeS-ATP-α-B (**7** and **8**):

$$^3J_{C6/8-H1'} = 4.5\cos^2(\chi - 60°) - 0.6\cos(\chi - 60°) + 0.1$$

$$^3J_{C2/4-H1'} = 4.7\cos^2(\chi - 60°) + 2.3\cos(\chi - 60°) + 0.1$$

The first equation provides values of $\chi = 228.2°$ for the A-isomer, and $\chi = 210.1°$ for B-isomer in χ_{anti} range. The second equation yields $\chi = 217.8°$, since the *J* values for both diastereoisomers are identical ($^3J_{C2/4-H1'} = 2$ Hz).

Sugar Puckering.

The conformation of the D-ribose ring of 2-MeS-ATP-α-B was analyzed in terms of a dynamic equilibrium between two favored puckered conformations: a type *N* conformer and a type *S* conformer.[12,13] *N* and *S* equilibrium populations were calculated from observed $J_{1'2'}$ and $J_{3'4'}$ couplings as reported previously.[14] According to this method, the observed vicinal couplings are related to the relative proportion of conformers by eqs 1−3:

$$J_{1'2'} = 9.3(1 - X_N) = 9.3X_S \quad (1)$$

$$J_{2'3'} = 4.6X_N + 5.3(1 - X_N) \quad (2)$$

$$J_{3'4'} = 9.3X_N \quad (3)$$

Table 1. Chemical Shifts and Splitting Pattern of 2-MeS-ATP-α-B in D_2O

isomer A	H8	H1′	H2′	H3′	H4′	H5′	H5″
chemical shift (δ)	8.46	6.14	4.82	4.69	4.38	4.35	4.14
coupling constants (Hz)	s	d 5.3	dd 5.3, 5.0	dd 5.0, 4.0	ddd 2.4, 2.8, 4.0	ddd 2.4, 4.2, 11.8	ddd 2.8, 4.5, 11.8
isomer B	H8	H1′	H2′	H3′	H4′	H5′	H5″
chemical shift (δ)	8.42	6.13	4.86	4.61	4.39	4.29	4.19
coupling constants (Hz)	s	d 5.7	dd 5.7, 5.1	dd 5.1, 3.7	ddd 2.9, 3.2, 3.7	ddd 3.2, 7.7, 11.8	ddd 2.9, 5.8, 11.8

Table 2. ^3J Coupling Constants (Hz) of 2-MeS-ATP-α-B in D_2O

	1′, 2′	2′, 3′	3′, 4′	4′, 5′	4′, ″5	5′, P_α	5″, P_α	C8, H1′	C4, H1′
isomer A	5.3	5.0	4.0	2.4	2.8	4.2	4.5	5	2
isomer B	5.7	5.1	3.7	3.2	2.9	7.7	5.8	4	2

Table 3. Conformational Analysis of 2-MeS-ATP-α-B in Solution

sugar pucker		C4′−C5′ bond		C5′−O5′ bond	
isomer A %	isomer B %	isomer A%	isomer B%	isomer A%	isomer B%
$X_S = 57.0$	$X_S = 60.6$	$gg = 88.4$	$gg = 79.1$	$gg = 73.3$	$gg = 48.2$
$X_N = 43.0$	$X_N = 39.4$	$tg = 3.7$	$tg = 12$	$tg = 12.6$	$tg = 30.9$
$K_{eq} = 1.32$	$K_{eq} = 1.54$	$gt = 7.9$	$gt = 8.9$	$gt = 14.1$	$gt = 20.9$

Scheme 4. Possible Nucleotide Rotamers: (A) Rotamers around the C4′−C5′ Bond and (B) Rotamers around the C5′−O5′ Bond

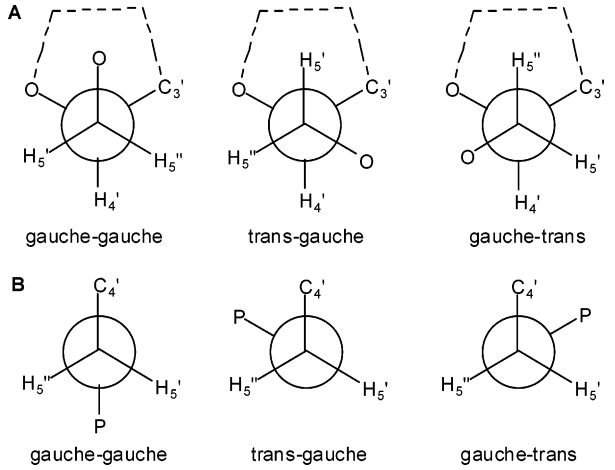

The equilibrium constant K_{eq} can be calculated directly from the observed values of $J_{1'2'}$ and $J_{3'4'}$:

$$K_{eq} = X_S/X_N = J_{1'2'}/J_{3'4'} \quad (4)$$

Using the assigned J-coupling constants (Table 2) and the above equation, the mole fraction of conformers S and N and K_{eq} for both diastereoisomers were calculated and the results are summarized in Table 3. For both A- and B-isomers the predominant ribose pucker is S (57% and 61% for A- and B-isomers, respectively).

Conformations of Exocyclic CH_2OR Group (R = Phosphate). 1. C4′−C5′ Bond. The coupling constants $J_{4'5'}$ and $J_{4'5''}$ can be interpreted in terms of three classical staggered rotamers shown in Scheme 4A with a preferred gauche−gauche (gg) conformation.[12] The mole fractions of each staggered rotamer of C4′−C5′ were calculated from the following expressions (5−7):

$$\rho_{gg} = [(J_t + J_g) - (J_{4'5'} + J_{4'5''})]/(J_t - J_g) \quad (5)$$

$$\rho_{tg} = (J_{4'5'} - J_g)/(J_t - J_g) \quad (6)$$

$$\rho_{gt} = (J_{4'5''} - J_g)/(J_t - J_g) \quad (7)$$

The coupling constants for pure rotamers were estimated as $J_g = 2.04$ Hz and $J_t = 11.72$ Hz from the appropriate Karplus relation.[15,12] The observed proton signals which are labeled H5′ and H5″ refer to downfield and upfield signals, respectively. From the results presented in Table 3, there is a marked preference for a gg rotamer about C4′−C5′ bond in both diastereoisomers.

The computations of conformational properties for exocyclic carbinol groups and furanose ring conformations suggest a destabilization of the gg conformer in a C2′-endo (S) pucker relative to a C3′-endo (N) pucker of the furanose ring.[16] Table 3 shows that as the S conformer population increases (57% for A-isomer and 60.6% for B-isomer), the gg conformer population decreases (88.4% and 79.1%, respectively).

2. C5′−O5′ Bond. Rotamer populations about C5′−O5′ are calculated from ^{31}P−H5′ and ^{31}P−H5″ coupling constants by procedures analogous to those used for C4′−C5′, using eqs 8−10:

$$\rho_{gg} = [(J_t + J_g) - (J_{P5'} + J_{P5''})]/(J_t - J_g) \quad (8)$$

$$\rho_{tg} = (J_{P5'} - J_g)/(J_t - J_g) \quad (9)$$

$$\rho_{gt} = (J_{P5''} - J_g)/(J_t - J_g) \quad (10)$$

Where $J_t = 20.9$ Hz and $J_g = 1.8$ Hz, as reported previously.[12] Relative rotamer populations were then calculated from observed J(HCOP) magnitudes (Table 3). Clearly, the two diastereoisomers have different conformational behavior around the C5′−O5′ bond, because of the asymmetric center present in P_α.

Assignment of the Absolute Configuration of the Chiral Probes. A difference in the chemical shift of H8 is observed between the two diastereoisomers of 2-MeS-ATP-α-B. The signal of H8 of B-isomer in the ^{1}H NMR spectra is more shielded than the signal of H8 of A-isomer due to the influence of the vicinal BH_3 group on P_α (8.46 vs 8.42 ppm). Because of the difference in torsion angle of the C5′−O5′ bond between isomer A and B, as shown above, P_α is much further away from H8 in A-isomer than in B-isomer (B-isomer is shown in Scheme 5). This small, although indicative, $\Delta\delta$ between H8 of isomers A and B may be explained in terms of

Table 4. Differences of Chemical Shifts ($\Delta\delta$ in ppm) between Adenine Nucleotides Mg^{2+} Complexes and Parent Compounds

ATP analogue	analogue no.	P_α	P_β	P_γ
ATP	**1**	0.33	2.44	0.51
2-MeSATP-α-B	**7**, **8**	1.96	2.72	1.06
2-MeSATP-α-S	**9**, **10**	2.14	2.25	0.78

Scheme 5. S_p Configuration Is Attributed to Diastereoisomer **8** (B-isomer)

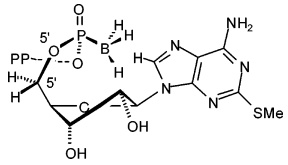

the greater proximity of the negative charge on BH_3 to H8 as compared to O. The greater proximity is due to the longer P−B bond (1.89 Å) as compared to P−O (1.60 Å), in addition to the contribution of the B−H bond (1.25 Å).[17] Furthermore, the upfield shift of H8 of the B-isomer may be due to an unconventional H-bond (known to exist between borane-amines and acidic protons)[18] between the BH_3 group and the relatively acidic H8.[8,19] Such a preferential intramolecular H-bond results in the shielding of H8.

Only in the *gt* rotamer is the BH_3 group near the H8 (population of this rotamer in B-isomer is higher than in A-isomer, 21% vs 14%). In the *gt* rotamer, the H8 is closer to the BH_3 group when P_α is in the S_p configuration with an expected H-bond length between H8 and BH_3 of ca. 1.9 Å[18] (Scheme 5).

Thus, the S_p configuration can be attributed to B-isomer, **8**, and R_p to A-isomer, **7**, of 2-MeS-ATP-α-B. Since the group priorities around P_α for ATP-α-S analogues are opposite to those of ATP-α-B, and assuming the same order of elution in HPLC, the absolute configuration assignments for 2-MeS-ATP-α-S analogues are that the S_p configuration is attributed to A-isomer, **9**, and R_p to B-isomer, **10**.

Indeed, this absolute configuration assignment was confirmed later by the biochemical assays and computational studies described below.

Coordination Analysis of Mg^{2+} Complexes of ATP and Analogues 7,8 and 9,10 in Solution. To learn the possible modes of coordination of Mg^{2+} with chiral probes **7**,**8** and **9**,**10** in solution, we explored the ^{31}P NMR spectra of these complexes at pH 7.4 and 0.04 M concentration of each nucleotide and $MgCl_2$ and compared the spectra to those of the ATP:Mg^{2+} complex (Table 4).

Apparently, all three phosphates in both chiral diastereoisomeric pair probes are involved in metal ion coordination, with P_β, being mostly affected. Yet, mixed chelate populations, i.e., $P_{\alpha,\beta}$-Mg^{2+} and $P_{\beta,\gamma}$-Mg^{2+} coordinated species, may exist at equilibrium. For ATP the effect of Mg^{2+} coordination is significantly lower at P_α and P_γ as compared to those values for analogues **7,8** and **9,10.**

Evaluation of Isomers of ATP-α-S (5,6) and 2-MeS-ATP-α-S (9,10) as $P2Y_1$-R Agonists. To study the efficacy of 2-MeS-ATP-α-S isomers **9**,**10**, we examined the $[Ca^{2+}]_i$ mobilization induced by these analogues and compared it to that of commercial S_p-ATP-α-S (**5**) and R_p-ATP-α-S (**6**) and ATP. These studies were performed in HEK cells that were stably transfected with $P2Y_1$ receptor. The density of the overexpressed $P2Y_1$-R is several orders of magnitude higher than that of the endogenous receptors. Therefore, the interaction of other P2Y-R subtypes with the tested ligands is negligible and does not contribute to the observed EC_{50} values.

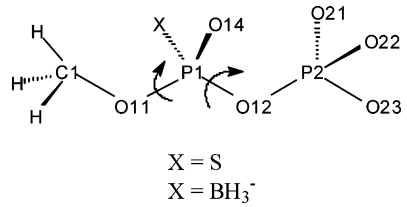

X = S
X = BH_3^-

Figure 5. Dihedral angles investigated during force field development for borano- or thiodiphosphate.

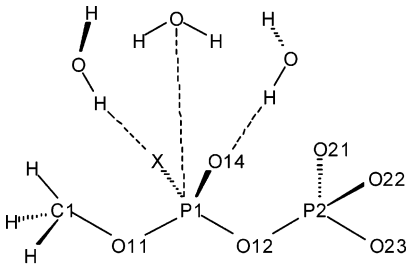

X = S
X = BH_3^-

Figure 6. Water−Me-boranodiphosphate or −Me-thiodiphosphate interaction geometries.

Table 5. Comparison of EC_{50} Values of Several ATP Analogues as $P2Y_1$-R Agonists

ATP analogue	analogue no.	absolute config	EC_{50} (nM)
ATP	**1**		590
2-MeS-ATP	**2**		1.0
ATP-α-B (A-isomer)	**3**	R_p	200
ATP-α-B (B-isomer)	**4**	S_p	>1000
ATP-α-S	**5**	S_p	9.4
ATP-α-S	**6**	R_p	75
2-MeS-ATP-α-B (A-isomer)	**7**	R_p	2.6
2-MeS-ATP-α-B (B-isomer)	**8**	S_p	53
2-MeS-ATP-α-S (A-isomer)	**9**	S_p	1.0
2-MeS-ATP-α-S (B-isomer)	**10**	R_p	20
2-Cl-ATP-α-B (A-isomer)	**11**	R_p	4.5
2-Cl-ATP-α-B (B-isomer)	**12**	S_p	36

Concentration−response curves of **9** and **10** show that both substances are more potent in inducing the $[Ca^{2+}]_i$ mobilization than ATP (Figure 3). The EC_{50} value of ATP is about 590 nM. However, the agonist effect of isomer **9** (EC_{50} 1 nM) is about 20-fold higher than that of its isomer **10** (EC_{50} 20 nM). 2-MeS-ATP is as potent as isomer **9** with a comparable EC_{50} value of 1 nM, Table 5 (curve not shown). The amplitude caused by 100 nM ATP was very small compared to the Ca^{2+} response caused by 1 μM ATP, which was close to the maximal response. The slopes for the concentration−response curves appear to differ between ATP and isomers **9/10**.

The concentration−response curves of the parent R_p-ATP-α-S and S_p-ATP-α-S isomers demonstrate that these two chiral analogues of ATP are more potent than ATP (Figure 4). In addition, isomer S_p-ATP-α-S (**5**) with an EC_{50} value of 9.4 nM is about 8-fold more potent than its isomer R_p-ATP-α-S (**6**) (EC_{50} 75 nM). Taken together,

Table 6. Comparison of Ab Initio and Empirical Interaction Energies (kcal/mol) and Geometries (Å) between Water and Me-Diphosphate (MePP),[a] Me-α-Thiodiphosphate (MeSPP), and Me-α-Boranodiphosphate (MeBPP)

	ab initio (HF/6-31G*)		CHARMM	
interaction	R_{min}	E_{min}	R_{min}	E_{min}
MePP P1−OW	−20.8	3.64	−19.9	3.51
MePP O13−HW	−23.2	1.73	−18.5	1.64
MePP O14−HW	−23.2	1.73	−18.5	1.64
MeSPP P1−OW	−17.7	4.13	−16.8	3.38
MeSPP SA−HW	−12.8	2.43	−10.6	2.14
MeSPP O14−HW	−22.5	1.76	−22.7	1.61
MeBPP P1−OW	−16.7	4.03	−17.9	3.43
MeBPP BA−HW	−12.8	1.82	−9.3	1.68
MeBPP O14−HW	−23.7	1.75	−22.4	1.61

[a] From ref 35.

isomer **9** is the most powerful analogue of ATP compared with the other three indicated substances; isomer **5** is second in potency between the studied phosphorothioate analogues of ATP with increased metabolic stability, indicating the role of the C2 methylthio ether moiety in enhancing affinity toward the $P2Y_1$-R. Isomers **10** and **6** are also good agonists of $P2Y_1$-R, but with lower potency in comparison with isomers **9** and **5**. Thus, the finding that S_p-ATP-α-S is more potent than its R_p counterpart supports our spectral assignment of the absolute configuration of 2-MeS-ATP-α-S isomers.

Molecular Modeling of the *h*-P2Y$_1$-R Agonists 1−12 and their Complexes with the Receptor. Overview. For the computational analysis of the chiral discrimination by the *h*-$P2Y_1$-R, ATP analogues **1**−**12** were employed as probe ligands.

Initially, the CHARMM 27 force field was augmented with new parameters for these novel ATP analogues, to enable reliable docking experiments. These parameters account for changes to the adenine ring due to C2-substituents[4] and changes to the phosphate chain due to P_α phosphorothioate and boranophosphate modifications.

Subsequently, the ATP analogues were docked into the receptor model to obtain information regarding the molecular recognition determinants at the *h*-$P2Y_1$-R binding site. Thereafter, we performed a quantitative estimation of the importance of specific H-bonding interactions employing quantum mechanical calculations on model compounds.

Phosphate Modifications. To generate parameters for the chiral P_α-ATP derivatives used in this study, methyl diphosphate (MePP) was used as a model compound.[35] Thus, to represent the P_α-phosphorothioate and P_α-boranophosphate functions, Me-P_α-thiodiphosphate (MeSPP) and Me-P_α-boranodiphosphate (MeBPP) were employed (Figure 5, see Methods). The interaction energies between MeSPP and MeBPP and individual water molecules were computed at the ab initio QM level and the CHARMM partial atomic charges were fitted to reproduce the interaction distances and energies (Figure 6). The interaction energies obtained using HF/6-31G* and the new CHARMM parameters are presented in Table 6. The values for MePP[35] are presented for comparison. The main difference is the considerably lower interaction energies in the diphosphate derivatives, where sulfur or BH_3^- participates in the hydrogen bonding. The interaction energies of these diphosphate derivatives are approximately half the energies of the parent compounds. Sulfur forms relatively weak H-bonds,[20] with a longer interaction distance than that of oxygen, and BH_3^- may participate in weak H-bonds as H-bond donors via the hydrogen atoms.[18] These results emphasize the lower potential of sulfur and BH_3^- compared to that of oxygen to participate in electrostatic interactions.

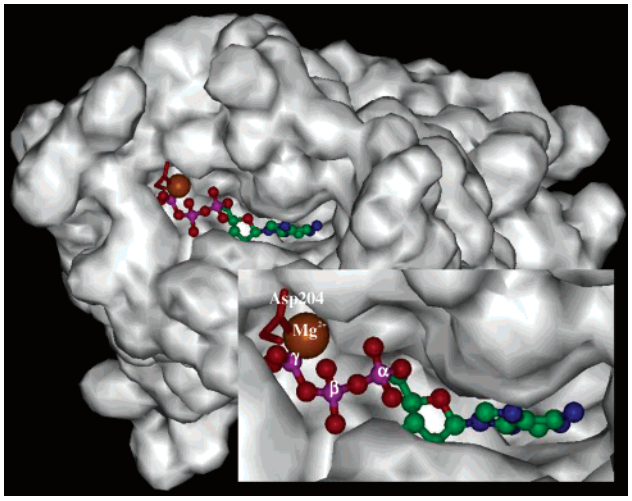

Figure 7. ATP docked into the binding pocket of the *h*-$P2Y_1$-R. A putative Mg^{2+} ion is coordinated to the phosphate moiety of ATP and to Asp204. Extracellular loops are deleted for clarity.

The CHARMM interaction distances and energies agree well with the ab initio results. The correlation coefficients, R^2, from a least-squares fit between ab initio QM and empirical data for MeSPP yield a perfect fit of 1 for both interaction distances and energies. For MeBPP, the interaction energy correlation coefficient drops to 0.89, while R^2 for the interaction distances is 1.

Docking Studies. The stereoelectronic recognition by the *h*-$P2Y_1$-R was investigated by docking ATP analogues **1**−**12**. These docking studies used the *h*-$P2Y_1$-R model described in the companion paper.[4] In this model, ATP is bound approximately 5 Å below the membrane plane and is involved in a multitude of interactions with the receptor. The phosphate chain is tightly bound by several positively charged amino acid residues, including Arg128, Lys280, and Arg310. The adenine moiety is more loosely bound, interacting with Arg310, Ser314, and possibly Tyr58. In this model, a Mg^{2+} ion was introduced into the binding site, to account for the diastereoselectivity observed for this receptor (see Discussion). A typical view of ATP docked into the receptor binding pocket with the Mg^{2+} coordinated by the phosphate moiety and Asp204 is presented in Figure 7. The ATP possibly coordinates with the Mg^{2+} ion via the α, *β*, and *γ* phosphates, supported by the above NMR analysis of Mg^{2+}−nucleotide complexes, with the free octahedral position of the Mg^{2+} ion probably occupied by a water molecule. Metal ion coordination with the ATP phosphates induces new chiral centers at the P atoms. The conformation around the α-phosphate of bound ATP may be defined as either pro-R_p or conversely as the Λ configuration (Scheme 6). Thus, according to the current *h*-$P2Y_1$-R model, the phosphate-Mg^{2+} configuration required for recognition by the receptor is Λ.

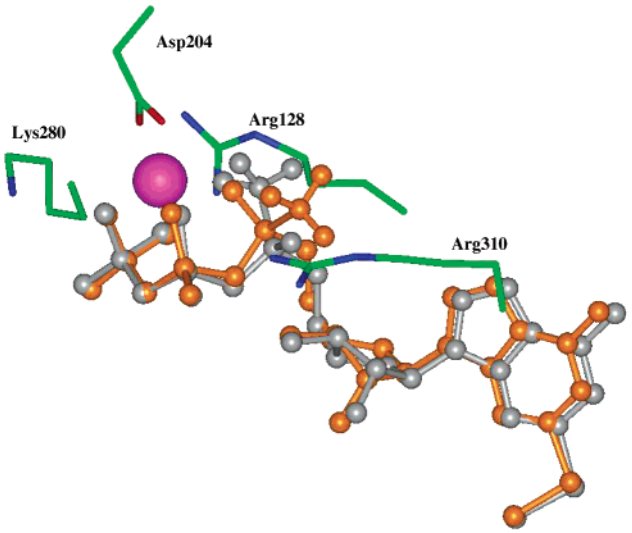

Figure 8. 2-MeS-α-B-ATP docked into the *h*-P2Y$_1$-R model: gold, R_p-isomer; silver, S_p-isomer. pink, Mg^{2+} ion.

Scheme 6. Screw Sense of Nucleotide−Mg^{2+} Complexes Used as Chiral Probes of P2Y$_1$-R

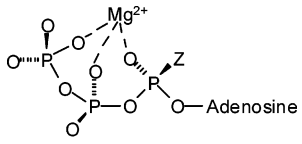

Z = O (Λ configuration, ATP)
Z = S (Λ configuration; **5**, **9**)
Z = BH_3 (Λ configuration; **3**, **7**)

Table 7. Interaction Energies[a] between the *h*-P2Y$_1$-R and Various ATP Derivatives

ATP and derivatives	analogue no.	Δ*E* (kcal/mol)
ATP	1	−1214.5 ± 12.5
2-MeS-ATP	2	−1218.7 ± 12.7
ATP-α-B (R_p-isomer)	3	−1220.0 ± 10.6
ATP-α-B (S_p-isomer)	4	−1180.3 ± 9.4
ATP-α-S (S_p-isomer)	5	−1237.1 ± 11.8
ATP-α-S (R_p-isomer)	6	−1188.7 ± 9.3
2-MeS-ATP-α-B (R_p-isomer)	7	−1221.2 ± 9.3
2-MeS-ATP-α-B (S_p-isomer)	8	−1182.6 ± 8.2
2-MeS-ATP-α-S (S_p-isomer)	9	−1236.4 ± 10.5
2-MeS-ATP-α-S (R_p-isomer)	10	−1193.2 ± 8.8
2-Cl-ATP-α-B (R_p-isomer)	11	−1222.3 ± 11.4
2-Cl-ATP-α-B (S_p-isomer)	12	−1177.0 ± 8.6

[a] The interaction energy was defined as $\Delta E_{inter} = \Delta E_{R\cdot L} - (E_R + E_L)$.

ATP derivatives **1**−**12** were docked into the *h*-P2Y$_1$-R model, using MC simulations. According to this scheme, some flexibility is added to binding-site side chains in addition to ligand flexibility. The interaction energy, which accounts for the nonbonded interactions between the receptor and the ligand, was employed as a crude estimate of the binding free energy. The average interaction energies obtained for ATP derivatives **1**−**12** over 100 000 steps of MC docking are presented in Table 7.

For the α-boranophosphate derivatives (**3**/**4**, **7**/**8**, **11**/**12**), the R_p-isomer displays the greatest interaction energy. On the other hand, for the α-phosphorothioate derivatives (**5**/**6**, **9**/**10**), the greatest interaction energies were obtained for the S_p-isomer. The common denominator for the α-boranophosphate R_p-isomers and the α-phosphorothioate S_p-isomers is that only the α-phosphate oxygen may participate in Mg^{2+} coordination and not the BH_3^- group or the sulfur atom, respectively. Thus, the docking experiments clearly demonstrate the chiral discrimination of the *h*-P2Y$_1$-R for one diastereomer. For instance, in the case of the R_p-isomer of 2-MeS-α-B-ATP (**7**) the coordination with Mg^{2+} is predicted to be with α, *β*, *γ*-phosphates (Figure 8). Thus, for the R_p diastereomer, interaction with the Mg^{2+} ion is maximized. However, in the case of the S_p-isomer (**8**), the ligand loses the coordination with the α-phosphate due to the lack of coordination of BH_3^- with Mg^{2+}. In this case, the coordination of the phosphate moiety with the Mg^{2+} ion is via *β*,*γ*-phosphates only. This loss of α-coordination with the Mg^{2+} ion considerably lowers the interaction energy of the S_p ligand with the receptor-Mg^{2+}, relative to the R_p-isomer. The same argument holds for the diastereomeric pairs of phosphorothioate analogues **5**/**6** and **9**/**10**. Here, the clear preference of Mg^{2+} for the "hard", namely, small and not easily polarizable, phosphate oxygen as opposed to the "soft" sulfur atom, large and fairly polarizable, accounts for the receptor's selectivity for the R_p-isomer.

Discussion

Conformational Changes of the ATP Analogue Are Induced upon Diffusion from the Solution to the P2Y$_1$-R Binding Pocket. Upon diffusion of 2-MeS-ATP-α-B (**7**, R_p-isomer) from the aqueous solution to its binding site within the *h*-P2Y$_1$-R, several conformational changes occur. Thus, this isomer, which in solution has a slight preference to the Southern ribose pucker (57%), transforms exclusively into the Northern conformation with a pseudorotation angle of 43.5° and ring puckering of 29.3°.[4] The predominant *gg* conformation around C4′−C5′ for **7** in solution (88%) is exclusively occupied in the P2Y$_1$-R with a value of −64.4° ± 9°.[4] Likewise, the *χ* angle around the glycosidic bond of **7** in solution remains practically the same as that of **7** in the receptor, 228° vs 239° ± 11°.

In this way, the P2Y$_1$-R ligand **7** acquires a more extended, elongated conformation upon binding to the receptor.

A Metal Ion Possibly Plays a Pivotal Role in the Chiral Discrimination of the *h*-P2Y$_1$-R. In this study we used chiral probes **3**−**12** to explore the diastereoselectivity of the *h*-P2Y$_1$-R. Indeed, these probes indicated a chiral discrimination by the receptor (Table 5). EC_{50} values for these analogues presented a 8−20-fold potency enhancement for one of the diastereoisomers as compared to their diastereoisomeric counterparts.

The absolute configuration assignment of our chiral probes necessitated X-ray crystal structure data for these analogues. Yet, due to the inherent difficulties in the crystallization of nucleotides, all our attempts to crystallize α-boranophosphate analogues **7** and **8** proved unsuccessful.

Alternatively, we applied an integrated approach combining $^1H/^{13}C$ NMR spectroscopy, biochemical assays, and molecular modeling for assigning the absolute configuration of analogues **3**−**4** and **7**−**12**.

The conformational analysis of 2-MeS-ATP-α-B isomers (**7**, **8**) in solution by NMR enabled the assignment of the R_p and S_p absolute configuration to isomer A and B (**7** and **8**), respectively (Scheme 5). Subsequently, the

absolute configuration of 2-MeS-ATP-α-S was obtained with A- and B-isomers (**9**, **10**) possessing the S_p and R_p configuration.

In the next phase, 2-MeS-ATP-α-S isomers with the above putative absolute configuration were evaluated as $P2Y_1$-R ligands in a functional assay. In addition, their EC_{50} values were compared to those of commercial ATP-α-S isomers, whose absolute configuration is known. The significantly higher potency of the S_p-isomer **9** as compared to R_p-isomer **10** (20-fold difference) was in accordance with that obtained for ATP-α-S S_p-isomer **5** vs R_p-isomer **6** (8-fold difference) (Table 5). This result supports our NMR analysis of the absolute configuration of ATP-α-B and ATP-α-S analogues.

Furthermore, computational docking studies indicated clearly for chiral probes **7,8** and **9,10** that only the R_p- and S_p-isomers of each, respectively, will form strong binding interactions, thus supporting the absolute configuration assignment mentioned above.

Finally, recent X-ray crystallography data for the NDPK-thymidine-α-borano-diphosphate complex[21] fully support our absolute configuration assignment.

For the elucidation of the origin of diastereoselectivity in the *h*-$P2Y_1$-R, we compared our biochemical and computational results with reports on the diastereoselectivity in nucleotide-binding enzymes.

The pivotal role of metal ions in determining the stereospecificity of enzymes was demonstrated in the classic report of Jaffe and Cohn.[22] In this work, diastereoisomers of ATP-α-S and ATP-*β*-S were used in combination with hard and soft metal ions. The preferential coordination of Mg^{2+} to oxygen and of Cd^{2+} to sulfur in the phosphorothioate analogues[23] resulted in the inversion of yeast hexokinase and rabbit muscle pyruvate kinase diastereomeric selectivity upon substituting Cd^{2+} for Mg^{2+} in the phosphoryl transfer reactions using a chiral ATP substrate (ATP-*β*-S).

The most common pattern, especially for kinases, seems to be a reversal of stereoselectivity with the ATP-*β*-S diastereoisomers coupled, with no reversal at the P_α. The results are usually interpreted as meaning that the *β*,*γ*-bidentate metal−nucleotide chelate is the active one in these enzyme-catalyzed reactions. Indeed, ATP−Mg^{2+} in kinases forms the *β*,*γ* bidentate chelate in the Λ screw sense.[24]

Therefore, the chiral discrimination we have observed by the $P2Y_1$-R for the diastereoisomers of ATP-α-B analogues[3] and for ATP-α-S analogues (Table 5) strongly supports the involvement of a metal ion as the origin of the receptor diastereoselectivity.

It is estimated that more than 90% of the ATP in cells is bound to Mg^{2+} ion.[25] In fact, because the intracellular Mg^{2+} concentration is generally an order of magnitude higher than the dissociation constant for MgATP, almost all intracellular ATP is complexed with Mg^{2+} (log stability constant for ATP^{4-} complex with Mg^{2+} is 4.29).[26] Since the concentration of extracellular Mg^{2+}, ca. 0.5−1 mM, is close to the intracellular concentration, ca. 0.25−1 mM,[27] we assume that extracellular ATP exists also mostly as the Mg^{2+} complex. The Mg^{2+} ion coordination occurs exclusively at the ATP's oxygen atoms, and not with N7, with water occupying the remaining octahedral positions about the metal.[25] Mg^{2+} can bind directly to the phosphate oxygen atoms (inner sphere coordination—the distance of metal−phosphorus is 3 Å) or via bridging water molecules (outer sphere coordination—the distance of metal−phosphorus is 6 Å).

Therefore, the ATP analogue bound to the $P2Y_1$-R is most likely metal ion bound, and the metal ion is most likely to be Mg^{2+}, although, to the best of our knowledge, no experimental evidence has been provided so far for the presence of a metal ion in the $P2Y_1$-R. Furthermore, in enzymes, metal ions, usually Mg^{2+}, play an important role in partially shielding the phosphate negative charges and aligning the substrate in proper orientation to produce the catalytic reaction.[26] In the $P2Y_1$-R, the putative Mg^{2+} ion can stabilize the ligand in a position so as to induce conformational changes of the receptor, in addition to neutralization of the ligand negative charges.

In ATP, various metal chelates of the α, *β*, and *γ* phosphate groups have been identified by X-ray crystallography and by ^{31}P NMR spectroscopy. Seven monodentate, bidentate, and tridentate metal−ATP isomers may form, including all of the permutations of α; *β*; *γ*; α,*β*; *γ*,*β*; α,*γ*; and α,*β*,*γ* coordination. Our ^{31}P NMR results for the Mg^{2+} complexes of chiral probes **7/8** and **9/10** indicate that in solution coordination involves all phosphates (Table 4). This could be either a simultaneous α,*β*,*γ* metal coordination or α,*β* and *β*,*γ* coordinated species existing in equilibrium. This finding is in agreement with earlier reports.[28]

The mode of ATP coordination with Mg^{2+} in the protein may be different than the mode in solution. For some proteins, the tridentate α,*β*,*γ* metal coordination complex is the active species, and for others, it is the bidentate *β*,*γ* complex.

Metal binding to the α- or *β*-phosphate groups of nucleotides imposes chirality on those phosphorus atoms. The bidentate *β*,*γ* Mg^{2+} complex has a chiral center on the P_β and the tridentate α,*β*,*γ* complex has chiral centers at both the P_α and the P_β. For the *β*,*γ*-bidentate chelate, the resulting two isomers have been designated Λ and Δ.

In our docking experiments, ATP putatively coordinates the Mg^{2+} ion via the α, *β*, and *γ* phosphates. Moreover, the computational results emphasize the receptor's preference for the Λ configuration. Therefore, the *h*-$P2Y_1$-R preferentially binds one diastereomer of ATP-α-S and ATP-α-B derivatives. In the case of the P_α-thiophosphate analogues, the S_p-isomer is predicted to be the more potent ligand, while for the P_α-boranophosphate derivatives, the R_p-isomer should be more potent, as was experimentally verified.

Here we found a difference of ca. 20-fold between the EC_{50} values of the diastereoisomer pairs of **7**,**8** and **9**,**10** (Table 5). This difference is apparently small as compared to up to several orders of magnitude in catalytic efficiency of various enzymes with pairs of substrate diastereoisomers.[22]

Indeed, small discriminatory preferences between diastereoisomers of ATP-α-S in enzymes are usually indicative of the involvement of P_α only in binding and not in catalysis. The changes in catalysis may be up to several orders of magnitude, whereas changes in kinetic parameters that are due to binding are around 1 order of magnitude.[5b] In our case, only binding plays a role

in the chiral discrimination, and this may explain a discrimination of ca. 20-fold between the diastereoisomers.

Therefore, we hypothesize that ATP-α-B and ATP-α-S analogues are recognized by the $P2Y_1$-R as follows: The Mg^{2+} ion that is held in the vicinity of the phosphate binding pocket by mono- or bidentate coordination with Asp204 coordinates also with the phosphate chain via P_α, P_β, and P_γ, with the remaining octahedral positions possibly occupied by water molecules (Figure 7). As the docking studies revealed, the required Mg^{2+}-phosphate configuration at the *h*-$P2Y_1$-R is the Λ configuration. Namely, for ATP, the pro-*R* oxygen atom will be coordinated preferentially to the pro-*S* oxygen atom.

The hard Mg^{2+} ion binds preferentially the hard oxygen atom rather than the soft sulfur atom in ATP-α-S analogues. Likewise, only the P_α oxygen atom in ATP-α-B analogues can coordinate with the metal ion. Thus, in the ATP-α-S (R_p) and ATP-α-B (S_p) isomers, the P_α oxygen is not in a position to coordinate the Mg^{2+} ion, and in this case the coordination is probably β,γ (Figure 8). Hence, these isomers lose a tight interaction with Mg^{2+} ion that has energetic implications and possibly also consequences for the orientation of the ligand, resulting eventually in their different EC_{50} values.

Our hypothesis regarding the $P2Y_1$-R origin of diastereoselectivity is supported by a recent related study on a complex of α-boranothymidine diphosphate with nucleoside diphosphate kinase (NDPK).[21] The 1.92 Å resolution crystal structure of the NDPK complex demonstrates that a Mg^{2+} ion ligates the α- and β-phosphates of the α-boranophosphate analogue, as observed for natural nucleotides, in addition to four water molecules. For the active α-borano thymidine diphosphate R_p-isomer, it was found that the α-borano group does not interact with the protein, and the metal ion coordination with the oxygen atoms of the phosphates is likely to determine the stereochemistry of recognition. Furthermore, the structures of our α,β,γ-Mg^{2+}-coordinated ligand−receptor complexes are supported by the crystal structure of 2′,3′-didehydro 2′,3′-dideoxythymidine triphosphate in NDPK. Here it was found that the Mg^{2+} ion coordinates with all three phosphates.

Conclusions

In this study, we observed a significant 20-fold difference in the potency of the diastereoisomers of both ATP-α-S and ATP-α-B analogues regarding the *h*-$P2Y_1$-R. We identified the absolute configuration of the potent *h*-$P2Y_1$-R ligands. Thus, it is the R_p ATP-α-B analogues **3**, **7**, and **11** and the S_p ATP-α-S analogues **5** and **9**, that induce higher affinity to the *h*-$P2Y_1$-R. Furthermore, we hypothesize that the $P2Y_1$-R's chiral discrimination originates from the requirement that the nucleotide analogue interacts with a Mg^{2+} ion within the receptor binding site. We identified the mode of coordination of the ATP analogues' triphosphate chain with a Mg^{2+} ion both in solution (experimentally) and in the receptor (computationally) and determined the active conformation as Λ. Furthermore, the conformational changes of the ligand occurring upon diffusion from the solution to the receptor's binding site were explained.

Methods

Synthesis. General. All air- and moisture-sensitive reactions were conducted in flame-dried, nitrogen-flushed, two-neck flasks sealed with rubber septa, and the reagents were introduced with a syringe. The progress of the reactions was monitored by TLC on precoated Merck silica gel plates (60F-254). Compounds were characterized by nuclear magnetic resonance using Bruker DMX-600, DPX-300, or AC-200 spectrometers. ^{1}H NMR spectra were measured in D_2O, and the chemical shifts are reported in ppm relative to HOD (4.78 ppm) as an internal standard. Nucleotides were characterized also by ^{31}P NMR in D_2O, using 85% H_3PO_4 as an external reference. Final products were characterized on an AutoSpec-E FISION VG high-resolution mass spectrometer desorbed from a glycerol matrix under FAB (fast atom bombardment) conditions. Primary purification of the nucleotides was achieved on an LC (Isco UA-6) system using a Sephadex DEAE-A25 column, which was swelled in 1 M $NaHCO_3$ in the cold for 1 day. Final purification of the nucleotides and separation of the diastereoisomer pair was achieved on a HPLC (Merck-Hitachi) system using a semipreparative reverse-phase column. Conditions for LC and HPLC separation are described below. The purity of the new nucleotides was determined on a Lichrospher 60 RP-select B column (250 × 4 mm) in the following solvent systems: system I, MeOH:0.1 M TEAA (triethylammonium acetate), 10:90 to 30:70 linear gradient in 25 min; system II, 5 mM TBAP (tetrabutylammonium dihydrogen phosphate) in MeOH:60 mM ammonium phosphate and 5 mM TBAP in 90% H_2O/10% MeOH, 10:90 to 40:60, linear gradient in 25 min. 2-Methylthioadenosine was synthesized from 2-SH-adenosine as described before.[29] 2-SH-adenosine was obtained from adenosine in three steps according to the procedure previously reported.[30]

Preparation of 2-Methylthioadenosine-5′-*O*-(α-*P*-thio)-triphosphate 9/10. 2-Methylthioadenosine-5′-*O*-(α-*P*-thio)-triphosphate was prepared according to our previously reported method.[6] The resulting residue was applied on an activated Sephadex DEAE-A25 column using a 0−0.6 M NH_4HCO_3 linear gradient (2000 mL). The relevant fractions were collected and freeze-dried, and excess NH_4HCO_3 was removed by repeated freeze-drying with deionized water to yield a mixture of **9** and **10** as a triammonium salt. Final purification and separation of diastereoisomers of 2-MeS-ATP-α-S was achieved on a semipreparative HPLC column. Subsequently, the triethylammonium counterions in each of the pure diastereoisomers were exchanged for Na^+ by passing the nucleotide through a Sephadex-CM C-25 column. Both diastereoisomers were obtained from 2-methylthioadenosine in 34% yield.

Reverse-Phase HPLC Separation of Diastereoisomers 9/10. The separation of diastereoisomers **9/10** was accomplished using a semipreparative reverse-phase Lichro CART 250−10 column and linear gradient [100 mM triethylammonium acetate (TEAA), pH 7 (A):MeOH (B), 90:10 to 70:30] for 25 min with flow rate of 5 mL/min. Fractions containing the same isomer (similar retention time) were freeze-dried. The excess buffer was removed by repeated freeze-drying with deionized water. The isomer with the shorter retention time (t_R) is designated isomer A and the other, isomer B.

2-SMe-ATP-α-S, 9 (A-Isomer). t_R: 15.26 min. ^{1}H NMR (D_2O, 300 MHz, Na^+ form): δ 8.50 (s, H-8, 1H), 6.12 (d, J = 5.8 Hz, H-1′, 1H), 4.88 (dd, J = 5.8, 5 Hz, H-2′, 1H), 4.66 (dd, J = 3.8, 5 Hz, H-3′, 1H), 4.40 (ddd, J = 3.8, 3.0, 3.1 Hz, H-4′, 1H), 4.34 (ddd, J = 3.1, 7.6, 11.7 Hz, H-5′, 1H), 4.26 (ddd, J = 3.0, 5.8, 11.7 Hz, H-5′, 1H), 2.58 (s, S−CH_3, 3H) ppm. ^{31}P NMR (D_2O, 81 MHz, Et_3N^+H form): δ 44.12 (d, J = 30.7 Hz, P_α), −10.26 (d, J = 21.2 Hz, P_γ), −23.64 (t, J = 21.4 Hz, P_β) ppm. UV: λ_{max} 275.7 nm. MS FAB (negative) *m*/*z*: 611.959 (M − 3H + 2Na)$^-$, 590.012 (M − 2H$^+$ + Na$^+$)$^-$, 568.023 (M − H)$^-$. t_R: 17.77 min (97.4% purity) using solvent system I. t_R: 17.75 min (95.9% purity) using solvent system II.

2-SMe-ATP-α-S, 10 (B-Isomer). t_R: 16.83 min. ^{1}H NMR (D_2O, 300 MHz, Na^+ form): δ 8.42 (s, H-8, 1H), 6.12 (d, J = 5.8 Hz, H-1′, 1H), 4.86 (dd, J = 5.8, 5.1 Hz, H-2′, 1H), 4.65

(dd, $J = 3.6, 5.1$ Hz, H-3′, 1H), 4.40 (ddd, $J = 2.9, 3.1, 3.6$ Hz, H-4′, 1H), 4.33 (ddd, $J = 2.9, 7.6, 11.7$ Hz, H-5′, 1H), 4.26 (ddd, $J = 3.1, 6.3, 11.7$ Hz, H-5′, 1H), 2.56 (s, S−CH_3, 3H) ppm. ^{31}P NMR (D_2O, 81 MHz, Et_3N^+H form): δ 43.87 (d, $J = 25.3$ Hz, P_α), −9.63 (d, $J = 16.3$ Hz, P_γ), −23.43 (t, $J = 23.2$ Hz, P_β) ppm. UV: λ_{max} 275.7 nm. MS FAB (negative) *m/z*: 611.978 $(M - 3H^+ + 2Na^+)^-$, 590.028 $(M - 2H^+ + Na^+)^-$, 568.034 $(M - H)^-$. t_R: 19.76 min (95.8% purity) using solvent system I. t_R: 17.68 min (91.2% purity) using solvent system II.

Biochemistry. Materials. Adenosine-5′-*O*-(1-thiotriphosphate), R_p-isomer (R_p-ATP-α-S), and adenosine-5′-*O*-(1-thiotriphosphate), S_p-isomer (S_p-ATP-α-S), were purchased from BIOLOG Life Science Institute (Bremen, Germany).

$[Ca^{2+}]_i$ Measurements. Transfection of HEK 293 cells with the $rP2Y_1$ receptor was carried out as described.[31] These HEK 293 cells were cultured on coverslips and used for pharmacological analysis.[32] For Ca^{2+} measurements, these HEK cells were loaded for 30 min with 2 μM Fura 2/AM in HEPES-buffered saline (HBS) containing 145 mM NaCl, 5.4 mM KCl, 1.8 mM $MgCl_2$, 25 mM glucose, and 20 mM HEPES, pH 7.4. Cells were assayed under continuous superfusion of 37 °C prewarmed HBS (2 mL/min) in the presence of varying concentrations of different nucleotides, as indicated.

The relative enzymatic stability of the analogues tested, in addition to the fast superfusion system used to apply the different ATP analogues, precludes any appreciable enzymatic conversion. Thus, problems related to responses that may result from degraded or released nucleotides are circumvented. Constant superfusion of the prewarmed buffer excluded unspecific Ca^{2+} responses caused by mechanical stress, temperature variation, or different components of the buffer.

Fluorescence changes of single cells were detected with an imaging system (TILL Photonics GmbH) attached to a Zeiss axioscope, using alternative excitation at 340/380 nm and emission at 510 nm. EC_{50} values were calculated from concentration−effect curves, as represented in Figures 3 and 4 and fitted with the Sigmaplot program. The data points in Figures 5 and 6 represent the mean ± SEM of 60−200 cells from at least three different experiments and two different preparations. Concentration−response data were analyzed with the Excel program applying $\Delta(F_{340nm}/F_{380nm})$ before and after the addition of the agonist. EC_{50} values represent the agonist concentration at which 50% of the maximal effect is achieved.

Computational Methods. Force Field Development. The CHARMM 27 force field[33−35] includes parameters for ATP. However, to describe the various ATP derivatives introduced in the current study, new parameters must be developed. Therefore, the CHARMM 27 force field was extended to include our ATP derivatives **2**−**12** that were investigated in the current docking studies. The CHARMM energy function is described by the following expression of internal and nonbonded terms:

$$V_T = \sum_{\text{bonds}} K_b(b - b_0)^2 + \sum_{\text{angles}} K_\theta(\theta - \theta_0)^2 + \sum_{\text{dihedrals}} K_\phi[1 + \cos(n\phi - \delta)]$$

$$+ \sum_{\text{1,3pairs}} K_{UB}(S - S_0)^2 + \sum_{\text{improper}} K_{imp}(\varphi - \varphi_0)^2$$

$$+ \sum_{\text{nonbonded}} \left(\epsilon_{ij} \left[\left(\frac{R_{\min,ij}}{r_{ij}} \right)^{12} - 2 \left(\frac{R_{\min,ij}}{r_{ij}} \right)^{6} \right] + \frac{q_i q_j}{4\pi D r_{ij}} \right)$$

In the above equation the first five terms relate to the internal energy, while the last two terms relate to the nonbonded energy. In the current study, only parameters for the dihedral and nonbonded terms were developed, since these are the only terms that are variable in the docking procedure. K_b, K_θ, K_{UB}, and K_{imp} are the bond, angle, Urey−Bradley, and improper dihedral force constants, respectively. b, θ, S, and φ are the bond length, bond angle, Urey−Bradley 1,3 distance, and improper dihedral angle, respectively. The subscript denotes equilibrium values. The torsional term is based on a cosine function, where K_ϕ is the force constant, n is the periodicity, and δ is the phase. The nonbonded terms are described by a Lennard-Jones term plus the Coulombic term. ϵ is the Lennard-Jones well depth, R_{min} is the distance at the Lennard-Jones minimum, and q_i is the partial atomic charge. A dielectric constant of unity was employed throughout.

The vdW parameters of sulfur were taken directly from the existing CHARMM parameters for sulfur, while for borane the recently developed parameters of Otkidach and Pletnev were used.[36] However, the vdW parameters for the borane hydrogens were optimized to fit ab initio interaction geometries and energies, as described below.

Initially, the MeSPP and MeBPP geometries were optimized at the quantum mechanical (QM) ab initio MP2/6-31+G* level.[37] For water, the TIP3 geometry was used.[38] Thereafter, the interaction energies between MeSPP or MeBPP and the water molecules were calculated at the HF/6-31G* level[39] and the CHARMM partial atomic charges were varied to obtain an optimal fit between the ab initio QM and empirical energies and interaction distances. In this case, no scaling of the ab initio energies was used.[35] Moreover, no diffuse functions were added to the 6-31G* basis set, to be consistent with previous work on MePP.[35]

Subsequently, we investigated the influence of substitution of the α-phosphate oxygen with either sulfur or BH_3^- on the rotation around the P−O bonds of the phosphate backbone (see Supporting Information). The PES map at the HF/6-31+G* level was compared with the one obtained using the existing dihedral parameters for MePP and the newly developed partial atomic charges for MeSPP and MeBPP. The force field PES map reproduced the main features of the ab initio surface and therefore the phosphate backbone dihedral angle parameters of MeSPP and MeBPP were set to those of MePP.

Docking Studies. The ATP derivatives addressed here were docked into the *h*-$P2Y_1$-R model developed in the companion paper.[4] In this model, the receptor is embedded in a fully hydrated lipid bilayer. However, for the current docking studies, the lipid bilayer and bulk water were not accounted for, since no changes to the receptor outside the binding site are performed.

Initially, the ligands were rigidly docked into the binding site using the location of ATP in our previous studies as a template.[4] Specifically, modifications to the ATP scaffold in its binding configuration were performed to obtain each of the derivatives **2**−**12**. Subsequently, the ligands were subjected to 100 000 steps of Monte Carlo (MC) simulations at 310 K. The docking studies employed MC simulations, where flexibility is added to the side chains that are in close proximity to the ligand.[4] The MC moves defined for the receptor were dihedral rotations around side chain bonds. Rigid rotations of the entire ligand of up to 30° and rigid translations of up to 0.5 Å were allowed per MC step, respectively. In addition, flexibility was added to all rotatable bonds within the ligand in addition to the rigid ligand rotations and translations. The complexation free energy was approximated crudely as the nonbonded interaction energy between ligand and receptor. Thus ligand desolvation, changes in internal energy, and entropy were ignored. However, here the main purpose of the interaction energy is to differentiate between different diastereomers, and a simple nonbonded interaction expression was deemed sufficient for this purpose.

A cutoff scheme of 8−12−13 Å was used for both electrostatics and vdW interactions in the simulations. Force and energy switching were used for electrostatic and vdW interactions, respectively.[40] This cutoff scheme entails turning on the switching functions at 8 Å, ignoring interactions beyond 12 Å, and keeping a list of all pair interactions within 13 Å.

All molecular mechanics calculations employed the CHARMM software package,[33] while all quantum mechanics computations used the Gaussian 98 program.[41]

Acknowledgment. This work was supported in part by BMBF-MOS, Grant No. 1812, and the Marcus Center

for Medicinal Chemistry. D.T.M. acknowledges the financial support provided by the Israeli Ministry of Science.

Supporting Information Available: Figures related to the CHARMM force field development and the partial atomic charges developed for derivatives **2**−**12** are provided. This material is available free of charge via the Internet at http://pubs.acs.org.

References

(1) (a) Fischer, B. Therapeutic Applications of ATP-(P2)-Receptors Agonists and Antagonists. *Exp. Opin. Therap. Pat.* **1999**, *9*, 385−399. (b) Guile, S. D.; Ince, F.; Ingall, A. H.; Kindon, N. D.; Meghani, P.; Mortimore, M. P. The Medicinal Chemistry of the P2 Receptor Family. *Prog. Med. Chem.* **2001**, *38*, 115−187. (c) Halbfinger, E.; Major, D. T.; Ritzmann, M.; Ubl, J.; Reiser, G.; Boyer, J. L.; Harden, K. T.; Fischer, B. Molecular Recognition of Modified Adenine Nucleotides by the $P2Y_1$-Receptor. 1. A Synthetic, Biochemical, and NMR Approach. *J. Med. Chem.* **1999**, *42*, 5325−5337. (d) Major, D. T.; Halbfinger, E.; Fischer, B. Molecular Recognition of Modified Adenine Nucleotides by the $P2Y_1$-Receptor. 2. A Computational Approach. *J. Med. Chem.* **1999**, *42*, 5338−5347. (e) Major, D. T.; Laxer, A.; Fischer, B. Protonation Studies of Modified Adenine and Adenine Nucleotides by Theoretical Calculations and ^{15}N NMR. *J. Org. Chem.* **2002**, *67*, 790−802.

(2) (a) Jacobson, K. A.; Jarvis, M. F.; Williams, M.Purine and Pyrimidine (P2) Receptors as Drug Targets *J. Med. Chem.* **2002**, *45*, 4057−4093. (b) van Rhee, A. M.; Fischer, B.; van Galen, P. J. M.; Jacobson, K. A. Modelling the P2Y Purinoceptor Using Rhodopsin As Template. *Drug Des. Discovery* **1995**, *13*, 133−154. (c) Moro, S.; Guo, D.; Camaioni, E.; Boyer, J. L.; Harden, T. K.; Jacobson, K. A Human P2Y(1) Receptor: Molecular Modeling and Site-Directed Mutagenesis as Tools to Identify Agonist and Antagonist Rrecognition Sites. *J. Med. Chem.* **1998**, *41*, 1456−1466. (d) Moro, S.; Hoffmann, C.; Jacobson, K. A. Role of the Extracellular Loops of G Protein-Coupled Receptors in Ligand Recognition: A Molecular Modeling Study of the Human P2Y(1) Receptor. *Biochemistry* **1999**, *38*, 3498−3509. (e) Kim, H. O.; Barak, D.; Harden, T. K.; Boyer, J. L.; Jacobson, K. A. Acyclic and Cyclopropyl Analogues of Adenosine Bisphosphate Antagonists of the P2Y(1) Receptor: Structure−Activity Relationships and Receptor Docking. *J. Med. Chem.* **2001**, *44*, 3092−3108.

(3) Nahum, V.; Zündorf, G.; Lévesque, S. A.; Beaudoin, A. R.; Reiser, G.; Fischer B. Adenosine 5′-*O*-(1-Boranotriphosphate) Derivatives as Novel $P2Y_1$ Receptor Agonists. *J. Med. Chem.* **2002**, *45*, 5384−5396.

(4) Major, D. T.; Fischer, B. Molecular Recognition in Purinergic Receptors. 1. A Comprehensive Computational Study of the *h*-$P2Y_1$-Receptor. *J. Med. Chem.* **2004**, *47*, 4391−4404.

(5) (a) Eckstein, F. Nucleoside Phosphorothioates. *Annu. Rev. Biochem.* **1985**, *54*, 367−402. (b) Garcia, G. A.; Leatherbarrow, R. J.; Eckstein, F.; Fersht, A. R. Metal-Ion Dependence of Phosphorothioate ATP Analogues in the Bacillus-Stearothermophilus Tyrosyl-Transfer RNA-Synthetase Reaction. *Biochemistry* **1990**, *29*, 1643−1648.

(6) Fischer, B.; Chulkin, A.; Boyer, J. L.; Harden, T. K.; Gendron, F.-P.; Beaudoin, A. R.; Chapal, J.; Hillaire-Buys, D.; Petit, P. 2-Thioether-5′-*O*-(1-thiotriphosphate) Adenosine Derivatives as New Insulin Secretagogues Acting Through P2Y-receptors. *J. Med. Chem.* **1999**, *42*, 3636−3646.

(7) Tulapurkar, M. E.; Laubinger, W.; Nahum, V.; Fischer, B.; Reiser, G. Subtype Specific Internalization of $P2Y_1$ and $P2Y_2$ Receptors Induced by Novel Adenosine 5′-O-(1-boranotriphosphate) Derivatives. *Br. J. Pharmacol.* **2004**, *142*, 869−878.

(8) Saenger W. In *Principles of nucleic acid structure*; Springer-Verlag: New York, 1984; pp 81−82.

(9) Donohue, J.; Trueblood, K. N. Base Pairing in DNA. *J. Mol. Biol.* **1960**, *2*, 363−371.

(10) Sundaralingam, M. Stereochemistry of Nucleic Acids and their Constituents. IV. Allowed and Preferred Conformations of Nucleosides, Nucleoside Mono-, Di-, Tri-, Tetraphosphates, Nucleic Acids, and Polynucleotides. *Biopolymers* **1969**, *7*, 821−860.

(11) Ippel, J. H.; Wijmenga, S. S.; de Jong, R.; Heus, H. A.; Hilbers, C. W. Heteronuclear Scalar Coupling in the Bases and Sugar Rings of Nucleic Acids: Their Determination and Application in Assignment and Conformational Analysis. *Magn. Reson. Chem.* **1996**, *34*, S156−S176.

(12) Davies, D. B.; Danyluk, S. S. Nuclear Magnetic Resonance Studies of 5′-Ribo- and Deoxyribonucleotide Structures in Solution. *Biochemistry* **1974**, *13*, 4417−4434.

(13) (a) Altona, C.; and Sundaralingam, M. Conformational Analysis of the Sugar Ring in Nucleosides and Nucleotides. New Description Using the Concept of Pseudorotation. *J. Am. Chem. Soc.* **1972**, *94*, 8205−8212. (b) Altona, C.; Sundaralingam, M. Conformational Analysis of the Sugar Ring in Nucleosides and Nucleotides. Improved Method for the Interpretation of Proton Magnetic Resonance Coupling Constants. *J. Am. Chem. Soc.* **1973**, 95, 2333−2344.

(14) Davies, D. B.; Danyluk, S. S. International Symposiuym on NMR Spectroscopy, University of Surrey, 1972.

(15) Blackburn, B. J.; Grey, A. A.; Smith, I. C. P.; Hruska, F. E. Determination of the Molecular Conformation of Uridine in Aqueous Solution by Proton Magnetic Resonance Spectroscopy. Comparison with β-Pseudouridine. *Can. J. Chem.* **1970**, *48*, 2866−2870.

(16) Hruska, F. E. In *Conformations of Biological Molecules and Polymers* (Proceedings of Jerusalem Symposium); Bergmann, E. D., Pullman, B., Eds.; Israel Academy of Science and Humanities: Jerusalem, 1973; p 345.

(17) Nahum, V. and Fischer, B. *Eur J. Inorg. Chem.* **2004**, in press.

(18) Fujii, A.; Patwari, G. N.; Ebata, T.; Mikami, N. Vibrational Spectroscopic Evidence of Unconventional Hydrogen Bonds. *Int. J. Mass Spect.* **2002**, *220*, 289−312.

(19) Srivastava, P. C.; Robins, R. K.; Meyer, R. B., Jr. In *Chemistry of nucleosides and nucleotides*; Townsend, L. B., Ed.; Plenum Press: New York, 1988; Vol. 1, pp 197−198.

(20) Platts, J. A.; Howard, S. T.; Bracke, B. R. F. Directionality of Hydrogen Bonds to Sulfur and Oxygen. *J. Am. Chem. Soc.* **1996**, *118*, 2726−2733.

(21) Meyer, P.; Schneider, B.; Sarfati, S.; Deville-Bonne, D.; Guerreiro, C.; Boretto, J.; Canard, B. Structural Basis for Activation of α-Boranophosphate Nucleotide Analogues Targeting Drug-resistant Reverse Transcriptase. *EMBO J.* **2000**, *19*, 3520−3529.

(22) Jaffe, E. K.; Cohn M. Divalent Cation-Dependent Stereospecifity of Adenosine 5′-O-(2-thiotriphosphate) in the Hexokinase and Pyrivate Kinase Reactions. The Absolute Stereochemistry of the Diastereoisomers of Adenosine 5′-O-(2-thiotriphosphate). *J. Biol. Chem.* **1978**, *253*, 4823−4825.

(23) Jaffe, E. K.; Cohn, M. 31P Nuclear Magnetic Resonance Spectra of the Thiophosphate Analogues of Adenine Nucleotides; Effects of pH and Mg^{2+} Binding. *J. Biol. Chem.* **1978**, *17*, 652−657.

(24) Romaniuk, P. J.; Eckstein, F. Structure of the Metal-Nucleotide Complex in the Acetate Kinase Reaction. A Study with gamma-^{32}P-labled Phosphorothioate analogues of ATP. *J. Biol. Chem.* **1981**, *256*, 7322−7328.

(25) Lippard, S. J.; Berg, J. M. In *Principles of Bioinorganic Chemistry*, University Science Books: Mill Valley, CA, 1994; pp 64−66, 132−133, 276−277.

(26) Klevickis & Grisham In *Metal ion in biological systems*; Sigel, A., Sigel, H., Eds.; Marcel Dekker: New York, 1996; Vol. 32.

(27) (a) Lane, M.; Boatman, D. E.; Albrecht, R. M.; Bavister, B. D. Intracellular Divalent Cation Homeostasis and Developmental Competence in the Hamster Preimplantation Embryo. *Mol. Reprod. Dev.* **1998**, *50*, 443−50. (b) Touyz, R. M.; Yao, G. Modulation of Vascular Smooth Muscle Cell Growth by Magnesium-role of Mitogen-Activated Protein Kinases. *J. Cell Physiol.* **2003**, *197*, 326−335. (c) Grubbs, R. D. Intracellular Magnesium and Magnesium Buffering. *BioMetals* **2002**, *15*, 251−259.

(28) Cohn, M. In *Biological actions of extracellular ATP*; Dubyak, G. R., Fedan, J. S., Eds.; Annals of the New York Academy of Sciences, Vol. 603; The New York Academy of Sciences: New York, 1990.

(29) Macfarlane, D. E. 2-Methylthioadenosine [β-^{32}P]diphosphate: Synthesis and Use as Probe of Platelet ADP Receptors. *Methods Enzymol.* **1992**, *215*, 137−142.

(30) (a) Kikugawa, K.; Suehiro, H.; Inchino, M. Platelet Aggregation Inhibitors. 6. 2-Thioadenosine Derivatives. *J. Med. Chem.* **1973**, *16*, 1381−1388. (b) Kikugawa, K.; Suehiro, H.; Yanase, R.; Aoki, A. Platelet Aggregation Inhibitors. IX. Chemical Transformation of Adenosine into 2-Thioadenosine Derivatives. *Chem. Pharm. Bull.* **1977**, *25*, 1959−1969.

(31) Vöhringer C, Schäfer R, Reiser G. A Chimeric Rat brain $P2Y_1$ Receptor Tagged with Green-Fluorescent Protein: High-Affinity Ligand Recognition of Adenosine Diphosphates and Triphosphates and Selectivity Identical to that of the Wild-Type Receptor. *Biochem. Pharmacol.* **2000**, *59*, 791−800.

(32) Zündorf, G.; Schäfer, R.; Vöhringer, C.; Halbfinger, E.; Fischer, B.; Reiser, G. Novel Modified Adenosine 5′-Triphosphate Analogues Pharmacologically Characterized in Human Embryonic Kidney 293 Cells Highly Expressing Rat Brain $P2Y_1$ Receptor: Biotinylated Analogue Potentially Suitable for Specific $P2Y_1$ Receptor Isolation. *Biochem. Pharmacol.* **2001**, *61*, 1259−1269.

(33) Brooks, B. R.; Bruccoleri, R. E.; Olafson, B. D.; States, D. J.; Swaminathan, S.; Karplus, M. CHARMM. A program for macromolecular energy, minimization, and dynamics calculations. *J. Comput. Chem.* **1983**, *4*, 187−217.

(34) Foloppe, N.; MacKerell, A. D., Jr. All-atom empirical force field for nucleic acids: I. Parameter optimization based on small molecule and condensed phase macromolecular target data. *J. Comput. Chem.* **2000**, *21*, 86−104.
(35) Pavelites, J. J.; Gao, J.; Bash, P. A.; Mackerell, A. D., Jr. A molecular mechanics force field for NAD(+), NADH, and the pyrophosphate groups of nucleotides. *J. Comput. Chem.* **1997**, *18*, 221−239.
(36) Otkidach, D. S.; Pletnev, I. V. Conformational analysis of boron-containing compounds using Gillespie-Kepert version of molecular mechanics. *J. Mol. Struct. (THEOCHEM)* **2001**, *536*, 65−72.
(37) Møller, C.; Plesset, M. S. Note on an approximate treatment for many-electron systems. *Phys. Rev.* **1934**, *46*, 618−622.
(38) Jorgensen, W. L.; Chandrasekhar, J.; Madura, J. D.; Impey, R. W.; Klein, M. L. Comparison of simple potential functions for simulating liquid water. *J. Chem. Phys.* **1983**, *79*, 926−935.
(39) (a) Hall, G. G. The molecular orbital theory of chemical valency VIII. A method for calculating ionisation potentials. *Proc. R. Soc, London Ser. A* **1951**, *205*, 541−552. (b) Roothan C. C. J. New developments in molecular orbital theory. *Rev. Mod. Phys.* **1951**, *23*, 69−89.
(40) Steinbach, P. J.; Brooks, B. R. New spherical-cutoff methods for long-range forces in macromolecular simulation. *J. Comput. Chem.* **1994**, *15*, 667−683.
(41) Frisch, M. J.; Trucks, G. W.; Schlegel, H. B.; Scuseria, G. E.; Robb, M. A.; Cheeseman, J. R.; Zakrzewski, V. G.; Montgomery, J. A.; Stratmann, R. E.; Burant, J. C.; Dapprich, S.; Millam, J. M.; Daniels, A. D.; Kudin, K. N.; Strain, M. C.; Farkas, O.; Tomasi, J.; Barone, V.; Cossi, M.; Cammi, R.; Mennucci, B.; Pomelli, C.; Adamo, C.; Clifford, S.; Ochterski, J.; Petersson, G. A.; Ayala, P. Y.; Cui, Q.; Morokuma, K.; Malick, D. K.; Rabuck, A. D.; Raghavachari, K.; Foresman, J. B.; Cioslowski, J.; Ortiz, J. V.; Stefanov, B. B.; Liu, G.; Liashenko, A.; Piskorz, P.; Komaromi, I.; Gomperts, R.; Martin, R. L.; Fox, D. J.; Keith, T.; Al-Laham, M. A.; Peng, C. Y.; Nanayakkara, A.; Gonzalez, C.; Challacombe, M.; Gill, P. M. W.; Johnson, B. G.; Chen, W.; Wong, M. W.; Andres, J. L.; Head-Gordon, M.; Replogle, E. S.; Pople, J. A. *Gaussian 98* (Revision A.7); Gaussian, Inc., Pittsburgh, PA, 1998.

JM049771U